

TRADI: Tracking deep neural network weight distributions

Gianni Franchi
SATIE, Université Paris-Sud
Université Paris-Saclay
gianni.franchi@u-psud.fr

Andrei Bursuc
valeo.ai
andrei.bursuc@valeo.com

Emanuel Aldea
SATIE, Université Paris-Sud
Université Paris-Saclay
emanuel.aldea@u-psud.fr

Séverine Dubuisson
CNRS, LIS
Aix Marseille University
severine.dubuisson@lis-lab.fr

Isabelle Bloch
LTCI, Télécom Paris
Institut polytechnique de Paris
isabelle.bloch@telecom-paris.fr

Abstract

During training, the weights of a Deep Neural Network (DNN) are optimized from a random initialization towards a nearly optimum value minimizing a loss function. Only this final state of the weights is typically kept for testing, while the wealth of information on the geometry of the weight space, accumulated over the descent towards the minimum is discarded. In this work we propose to make use of this knowledge and leverage it for computing the distributions of the weights of the DNN. This can be further used for estimating the epistemic uncertainty of the DNN by sampling an ensemble of networks from these distributions. To this end we introduce a method for tracking the trajectory of the weights during optimization, that does not require any changes in the architecture nor on the training procedure. We evaluate our method on standard classification and regression benchmarks, and on out-of-distribution detection for classification and semantic segmentation. We achieve competitive results, while preserving computational efficiency in comparison to other popular approaches.

1. Introduction

In recent years, Deep Neural Networks (DNNs) have achieved remarkable results in various computer vision tasks. Although the actual optimization process is well understood, much less is known about effective regularization and about the characterization of the convergence results, since non-convex cost functions lead to loss surfaces in high dimensional spaces with many local minima. The studies of the convergence of DNNs and their optimization in the light of reaching interesting local minima have been conducted on a variety of works [5, 42, 23]. In this article, we focus on interpreting the result of a DNN training process by track-

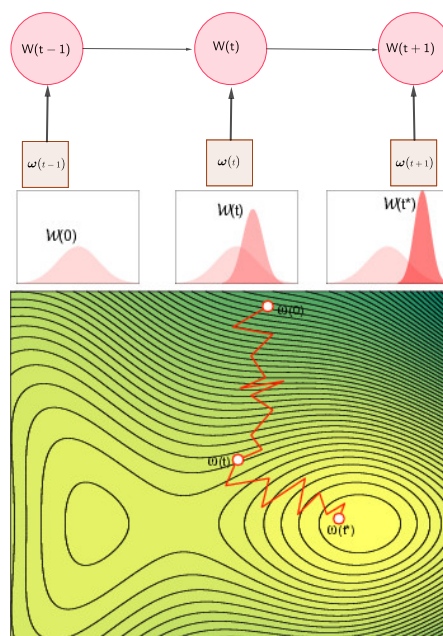


Figure 1: Our algorithm uses Kalman filtering in order to track during training, for all DNN neurons, the weight distribution \mathcal{W} from a generic prior $\mathcal{W}(0)$ to the final estimate $\mathcal{W}(t^*)$. We also estimate the covariance matrix of all the trainable network parameters. Popular alternative approaches rely typically either on ensembles of models trained independently [26] with a significant computational cost, approximate ensembles [9] or on averaging weights collected on different local minima [31].

ing the distribution of the network weights as the network structure emerges during learning.

Modern deep learning networks have good accuracy, however the learnt representation might be overconfident

on ambiguous instances bordering two classes (e.g., human wearing a cat costume), or on unrelated instances (e.g. plastic bag classified with high probability as rock). Knowledge about the distribution of the network weights during training opens an avenue for studying the evolution of the underlying covariance matrix, and the uncertainty of the model parameters, referred to as the epistemic uncertainty [22]. This uncertainty is due to the inherently limited data and knowledge available during training, and its evaluation is of crucial importance. Works in [15, 11] focus on proposing effective distributions for the initialization of the DNN weights. Then, by assuming that weights follow a Gaussian distribution at time $t = 0$, owing to the central limit theorem we know that weights will also converge to a Gaussian distribution. Hence, one needs to track during training only the mean and covariance of the weights in order to determine their distribution. To this effect, Kalman filtering [12] is an appropriate strategy for tractability reasons, as well as for the guaranteed optimality as long as the underlying assumptions are valid (linear dynamic system with Gaussian assumption in the predict and update steps). To the best of our knowledge, our work is the first attempt to use such technique to track the DNN weight distribution, and subsequently to estimate its epistemic uncertainty. Our technique can be extended to any training algorithm and any architecture model. At its core, it relies on a well-grounded method which is at the same time simple and straightforward to deploy in a tracking algorithm. In our experiments, we underline that the weight distribution provides new, effective statistics related to the uncertainty of the DNN during training, and relevant for regression tasks for which we achieve state of the art results.

Contributions. The keypoints of our contribution are: (a) this is the first work which filters in a tractable manner the trajectory of the entire set of trainable parameters of a DNN during the training process (b) the paper proposes as well a tractable approximation for estimating the covariance matrix of the network parameters (c) we achieve competitive or state of the art results on most regression datasets, and on out-of-distribution experiments on the AUPR-Error metric. We propose a framework that can be easily plugged into existing architectures and which is an effective indicator for the epistemic uncertainty of the considered model.

2. Related work

Uncertainty estimation is an important aspect for any machine learning model and it has been thoroughly studied across years in statistical learning areas. In the context of DNNs a renewed interest has surged in dealing with uncertainty in recent years, due to both the increasing effectiveness and popularity of such models, and their reputation as hard to interpret black models. In the following we briefly review methods related to our approach.

Bayesian methods. Bayesian approaches deal with uncertainty by identifying a distribution of the parameters of the model. The current posterior distribution is computed from a prior distribution assumed over the parameters and the likelihood of the model for the current data. The posterior is iteratively updated across training samples. The predictive distribution is then computed through Bayesian model averaging by sampling models from the posterior. This simple formalism is at the core of many machine learning models, including neural networks. Early approaches from Neal [33] leveraged Markov chain Monte Carlo variants for inference on Bayesian Neural Networks. However on modern multi-million parameter DNNs, such methods are computationally intractable for computing the posterior, leaving the lead to gradient based methods.

Modern Bayesian Neural Networks (BNNs). Progress in variational inference has enabled a revival of BNNs in recent years. Most notably, Kingma and Welling [24] introduce the reparameterization trick for training deep latent variable models and allowing backpropagation through learned distributions Blundell *et al.* [4] extend it to learn distributions over neurons via a Gaussian mixture prior. While such models are computationally appealing and easy to reason along, this type of methods are limited to small to medium networks, in particular MLPs. Gal and Ghahramani [9] suggest that Dropout [40] can be used to mimic a BNN by sampling different subsets of neurons at each forward pass during test time and use them as ensembles. Multiple MC Dropout variants and extensions have been subsequently proposed: for learning the dropout probability [10], introducing stochasticity through BatchNorm layers [41], heteroscedastic Dropout [27]. MC Dropout is currently the most popular instance of BNNs due to its speed and simplicity. However, the benefits of Dropout are more limited on convolutional layers and specific architectural design choices must be made on such networks, e.g. placing Dropout only next to a specific set of layers [21, 32]. The main criticisms of MC Dropout concern the fact that its uncertainty is not reducing with more training steps [34, 35], in which case ensembles would be preferable. Our approach is compatible with both fully-connected and convolutional layers, while our uncertainty estimates are expected to improve with training as we are relying on the Kalman filter formalism.

Ensemble Methods. Ensemble methods are arguably the top performers for measuring epistemic uncertainty, and are largely applied to various areas, e.g., active learning [3]. Lakshminarayan *et al.* [26] propose using an ensemble of DNNs with different random seeds at initialization and trained over the same data. The major drawback of this method is its computational cost since one has to train multiple DNNs, a cost which is particularly high in the case of typical architectures used for computer vision tasks, e.g. se-

mantic segmentation [8, 46]. Izmailov *et al.* [19] collect weight snapshots from different local minima in the final optimization part and average the weights to get an ensemble behavior of the final network corresponding to a wider and more robust optimization minimum. Maddox *et al.* [31] further extend this idea by fitting a distribution over the weights collected at multiple local minima and sample networks from this distribution at test time. Although this approach is less computationally intensive, the limitation of these methods is that the observations from these local minima are relatively sparse for such a high dimensional space and are less likely to capture the true distributions of the space around these weights. With TRADI we are mitigating these points as we collect statistics for the distribution of the weights at each step of the Stochastic Gradient Descent (SGD) optimization. Furthermore, our algorithm has a lighter computational cost than [26] during training.

Kalman filtering. The Kalman filter [20] is a recursive estimator that constructs an inference of unknown variables given measurements over time. With the advent of effective DNNs, researchers have tried integrating ideas from Kalman filtering in DNN training: for SLAM using RNNs (*e.g.*, IONet [7], BackpropKF [14]), improving optimization (*e.g.*, Batch Kalman Normalization [43]), or differentiable fusion of predictions from different networks [30]. In our approach, we employ Kalman filtering for keeping track of the statistics of the network during training such that at “convergence” we have a better coverage of the distribution around each parameter of a multi-million parameter DNN. The Kalman filter provides a clean and relatively easy to deploy formalism to this effect.

Weight initialization and optimization. Most of the initialization techniques [11, 15] of DNNs start with weights that are i.i.d samples from a Normal distribution. At each layer the samples are further scaled with factors depending on the number of input and output units, and on the downstream activation function. Batch Normalization [18], a highly effective optimization and regularization technique for DNNs, enforces a Normal distribution of intermediate activations at each layer leading to more stable activations and facilitating higher learning rates and faster convergence. WeightNormalization [39] has a similar effect over the weights at each layer making sure they are sticking to the initial distributions. From a Bayesian perspective the L_2 regularization, known as weight decay, is equivalent to putting a Gaussian prior over the weights. In our approach, we consider a prior over the weights, however we use it only in the filtering in order to reduce any major drifts in the estimations of distributions of the weights across training, while potentially mitigating instabilities that can happen in SGD steps (in particular in first steps with high learning rates).

3. TRacking of the weight DIstribution (TRADI)

In this section, we detail our approach aiming to first estimate the distribution of the weights of a DNN at each time step during optimization in the training phase, and then to generate an ensemble of networks by sampling from the computed distributions.

3.1. Notations and hypotheses

- X and Y are two random variables, with $X \sim \mathcal{P}_X$ and $Y \sim \mathcal{P}_Y$. Without loss of generality we consider the observed samples $\{x_i\}_{i=1}^n$ and the corresponding labels $\{y_i\}_{i=1}^n$ as vectors. From this set of observations, we derive a training set of n_l elements and a testing set of n_τ elements: $n = n_l + n_\tau$.
- Training/Testing sets are denoted respectively by $\mathcal{D}_l = (x_i, y_i)_{i=1}^{n_l}$, $\mathcal{D}_\tau = (x_i, y_i)_{i=1}^{n_\tau}$. Data in \mathcal{D}_l and \mathcal{D}_τ are assumed to be i.i.d. distributed according to their respective unknown joint distribution \mathcal{P}_l and \mathcal{P}_τ .
- The DNN is defined by a vector containing the K trainable weights $\omega = \{\omega_k\}_{k=1}^K$. During training, ω , is iteratively updated for each mini-batch and we denote by $\omega(t)$ the state of the DNN at iteration t of the optimization algorithm, and following the random variable $W(t)$. g represents the architecture of the DNN associated with these weights and $g_{\omega(t)}(x_i)$ its output at t . $\omega(0)$ is the initial set of weights $\{\omega_k(0)\}_{k=1}^K$ following $\mathcal{N}(0, \sigma_k^2)$, where σ_k^2 are fixed as in [15].
- $\mathcal{L}(\omega(t), y_i)$ is the loss function used to measure the dissimilarity between the output $g_{\omega(t)}(x_i)$ of the DNN and the expected output y_i . Different loss functions can be considered according to the type of task.
- Weights on different layers are assumed to be independent of one another at all times. Each weight $\omega_k(t)$, $k = 1, \dots, K$, follows a non-stationary Normal distribution (*e.g.*, $W_k(t) \sim \mathcal{N}(\mu_k(t), \sigma_k^2(t))$) whose two parameters are tracked.

3.2. TRacking of the DIstribution (TRADI) of weights of a DNN

3.2.1 Tracking the mean and variance of the weights

DNN optimization typically starts from a set of randomly initialized weights $\omega(0)$. Then, at each training step t , several SGD updates are performed from a randomly chosen mini-batch towards minimizing the loss. This makes the trajectory of the weights vary, but not necessarily in the good direction each time [28]. Since gradients are averaged over mini-batches, we can consider that weight trajectories are averaged over each mini-batch. After a certain number of

epochs, the DNN converges, *i.e.*, it reaches a local optimum with a specific configuration of weights that will then be used for testing. However, this general approach for training does not consider the evolution of the distribution of the weights, which may be estimated from the training trajectory and from the dynamics of the weights over time. In our work, we argue that the history of the weight evolution up to their final state is an effective tool for estimating the epistemic uncertainty, *i.e.*, the model uncertainty.

More specifically, our goal is to estimate, for all weights $\omega_k(t)$ of the DNN and at each training step t , $\mu_k(t)$ and $\sigma_k^2(t)$, the parameters of their normal distribution. Furthermore, for small networks we can also estimate the covariance $\text{cov}(W_k(t), W_{k'}(t))$ for any pair of weights $(\omega_k(t), \omega_{k'}(t))$ at t in the DNN (see supplementary material for details). To that end, we leverage mini-batch SGD in order to optimize the loss between two weight realizations. The loss derivative with respect to a given weight $\omega_k(t)$ over a mini-batch $B(t)$ is given by:

$$\nabla \mathcal{L}_{\omega_k(t)} = \frac{1}{|B(t)|} \sum_{(x_i, y_i) \in B(t)} \frac{\partial \mathcal{L}(\omega(t-1), y_i)}{\partial \omega_k(t-1)} \quad (1)$$

Weights $\omega_k(t)$ are then updated as follows:

$$\omega_k(t) = \omega_k(t-1) - \eta \nabla \mathcal{L}_{\omega_k(t)} \quad (2)$$

with η the learning rate.

The weights of DNNs are randomly initialized at $t = 0$ by sampling $W_k(0) \sim \mathcal{N}(\mu_k(0), \sigma_k^2(0))$, where the parameters of the distribution are set empirically on a per-layer basis [15]. By computing the expectation of $\omega_k(t)$ in Equation (2), and using its linearity property, we get:

$$\mu_k(t) = \mu_k(t-1) - \mathbb{E} [\eta \nabla \mathcal{L}_{\omega_k(t)}] \quad (3)$$

We can see that $\mu_k(t)$ depends on $\mu_k(t-1)$ and on another function at time $t-1$: this shows that the means of the weights follow a Markov process.

As in [2, 45] we assume that weights during back-propagation and forward pass are independent. We then get:

$$\sigma_k^2(t) = \sigma_k^2(t-1) + \eta^2 \mathbb{E} [(\nabla \mathcal{L}_{\omega_k(t)})^2] - \eta^2 \mathbb{E}^2 [\nabla \mathcal{L}_{\omega_k(t)}] \quad (4)$$

This leads to the following state and measurement equations for the mean $\mu_k(t)$:

$$\begin{cases} \mu_k(t) = \mu_k(t-1) - \eta \nabla \mathcal{L}_{\omega_k(t)} + \varepsilon_\mu \\ \omega_k(t) = \mu_k(t) + \tilde{\varepsilon}_\mu \end{cases} \quad (5)$$

with ε_μ being the state noise, and $\tilde{\varepsilon}_\mu$ being the observation noise, as realizations of $\mathcal{N}(0, \sigma_\mu^2)$ and $\mathcal{N}(0, \tilde{\sigma}_\mu^2)$ respectively. The state and measurement equations for the variance σ_k are given by:

$$\begin{cases} \sigma_k^2(t) = \sigma_k^2(t-1) + (\eta \nabla \mathcal{L}_{\omega_k(t)})^2 - \eta^2 \mu_k(t)^2 + \varepsilon_\sigma \\ z_k(t) = \sigma_k^2(t) - \mu_k(t)^2 + \tilde{\varepsilon}_\sigma \\ \text{with } z_k(t) = \omega_k(t)^2 \end{cases} \quad (6)$$

with ε_σ being the state noise, and $\tilde{\varepsilon}_\sigma$ being the observation noise, as realizations of $\mathcal{N}(0, \sigma_\sigma^2)$ and $\mathcal{N}(0, \tilde{\sigma}_\sigma^2)$, respectively.

3.2.2 Approximating the covariance

Using the measurement and state transition equations (5) and (6), we can apply a Kalman filter to track the state of each trainable parameter. As the computational cost for tracking the covariance matrix is significant, we propose to track instead only the variance of the distribution. We propose here to approximate the covariance by employing a model inspired from Gaussian Processes [44]. We consider the Gaussian model due to its simplicity and good results. Let us denote $\Sigma(t)$ the covariance of $W(t)$, and let $\mathbf{v}(t) = (\sigma_0(t), \sigma_1(t), \sigma_2(t), \dots, \sigma_K(t))$ be a vector of size K composed of the standard deviations of all weights at time t . The covariance matrix is approximated by $\hat{\Sigma}(t) = (\mathbf{v}(t)\mathbf{v}(t)^T) \odot \mathcal{K}(t)$, where \odot is the Hadamard product, and $\mathcal{K}(t)$ is the kernel corresponding to the $K \times K$ Gram matrix of the weights of the DNN, in which the coefficient (k, k') is given by $\mathcal{K}(\omega_k(t), \omega_{k'}(t)) = \exp\left(-\frac{\|\omega_k(t) - \omega_{k'}(t)\|^2}{2\sigma_{\text{rbf}}^2}\right)$. The computational cost for storing and processing the kernel $\mathcal{K}(t)$ is however prohibitive in practice as its complexity is quadratic in terms of the number of weights, which may reach, for recent DNNs, $K \approx 10^9$.

Rahimi and Recht [38] alleviate this problem by approximating non-linear kernels, *e.g.*, Gaussian RBF, in an unbiased way using random feature representations. Then, for any translation-invariant positive definite kernel $\mathcal{K}(t)$, $\forall (\omega_k(t), \omega_{k'}(t))$, $\mathcal{K}(\omega_k(t), \omega_{k'}(t))$ depends only on $\omega_k(t) - \omega_{k'}(t)$. We can then approximate the matrix by:

$$\mathcal{K}(\omega_k(t), \omega_{k'}(t)) \equiv \mathbb{E} [\cos(\Theta \omega_k(t) + \Phi) \cos(\Theta \omega_{k'}(t) + \Phi)]$$

where $\Theta \sim \mathcal{N}(0, \sigma_{\text{rbf}}^2)$ (this distribution is the Fourier transform of the kernel distribution) and $\Phi \sim \mathcal{U}_{[0, 2\pi]}$. In detail, we approximate the high-dimensional feature space by projecting over the following N -dimensional feature vector:

$$\mathbf{z}(\omega_k(t)) \equiv \sqrt{\frac{2}{N}} [\cos(\theta_1 \omega_k(t) + \phi_1), \dots, \cos(\theta_N \omega_k(t) + \phi_N)]^\top \quad (7)$$

where the $\theta_1, \dots, \theta_N$ are i.i.d from $\mathcal{N}(0, \sigma_{\text{rbf}}^2)$ and ϕ_1, \dots, ϕ_N are i.i.d from $\mathcal{U}_{[0, 2\pi]}$. In this new feature space we can approximate kernel $\mathcal{K}(t)$ by $\hat{\mathcal{K}}(t)$ defined by:

$$\hat{\mathcal{K}}(\omega_k(t), \omega_{k'}(t)) = \mathbf{z}(\omega_k(t))^\top \mathbf{z}(\omega_{k'}(t)) \quad (8)$$

Furthermore, [38] prove that the probability of having an error of approximation greater than $\epsilon \in \mathbb{R}^+$ depends on $\exp(-N\epsilon^2)/\epsilon^2$. To avoid the Hadamard product of matrices of size $K \times K$, we evaluate $\mathbf{r}(\omega_k(t)) = \sigma_k(t) \mathbf{z}(\omega_k(t))$, and the value at index (k, k') of the approximate covariance matrix $\hat{\Sigma}(t)$ is given by:

$$\hat{\Sigma}(t)(k, k') = \mathbf{r}(\omega_k(t))^\top \mathbf{r}(\omega_{k'}(t)). \quad (9)$$

3.3. Training the DNNs

In our approach, for classification we use the cross-entropy loss to get the log-likelihood similarly to [26]. For regression tasks, we train over two losses sequentially and modify $g_{\omega(t)}(x_i)$ to have two output heads: the classical regression output $\mu_{\text{pred}}(x_i)$ and the predicted variance of the output σ_{pred}^2 . This modification is inspired by [26], who propose having two outputs. The first loss is the MSE $\mathcal{L}_1(\omega(t), y_i) = \|g_{\omega(t)}(x_i) - y_i\|_2^2$ as used in the traditional regression tasks. The second loss is the negative log-likelihood (NLL) [26] which reads:

$$\mathcal{L}_2(\omega(t), y_i) = \frac{\|\mu_{\text{pred}}(x_i) - y_i\|_2^2}{2\sigma_{\text{pred}}(x_i)^2} + \frac{1}{2} \log(\sigma_{\text{pred}}(x_i)^2) + \text{cst} \quad (10)$$

We first train with loss $\mathcal{L}_1(\omega(t), y_i)$ until reaching a satisfying $\omega(t)$. In the second stage we add the variance prediction head and start fine-tuning from $\omega(t)$ with loss $\mathcal{L}_2(\omega(t), y_i)$. During our training of the original log-likelihood loss we have found it unstable, due to the logarithm non linearity. Hence, our sequential training is the key for having a more stable training.

3.4. TRADI training algorithm overview

We detail the TRADI steps during training in Algorithm 2. For tracking purposes we must store $\mu_k(t)$ and $\sigma_k(t)$ for all the weights of the network. Hence, we are computationally lighter than Deep Ensembles, which has a training complexity scaling with the number of considered models. In addition, TRADI can be applied to any DNN without any modification of the architecture, contrarily to MC dropout that requires adding dropout layers to the underlying DNN. For clarity we define $\mathcal{L}(\omega(t), B(t)) = \frac{1}{|B(t)|} \sum_{(x_i, y_i) \in B(t)} \mathcal{L}(\omega(t), y_i)$. Here $\mathbf{P}_\mu, \mathbf{P}_\sigma$ are the noise covariance matrices of the mean and variance respectively and $\mathbf{Q}_\mu, \mathbf{Q}_\sigma$ are the optimal gain matrices of the mean and variance respectively. These matrices are used during Kalman filtering [20].

3.5. TRADI uncertainty during testing

After having trained a DNN, we can evaluate its uncertainty by sampling new realizations of the weights from to the tracked distribution. We call $\tilde{\omega}(t) = \{\tilde{\omega}_k(t)\}_{k=1}^K$ the vector of size K containing these realizations. Note this vector is different from $\omega(t)$ since it is sampled from the distribution computed with TRADI, that does not correspond exactly to the DNN weight distribution. In addition, we note $\boldsymbol{\mu}(t)$ the vector of size K containing the mean of all weights at time t .

Then, two cases can occur. In the first case, we have access to the covariance matrix of the weights (by tracking or

Figure 2: TRADI algorithm during training

```

1:  $\omega(t)$ : weights,  $\eta$  learning rate,  $\sigma_\mu, \tilde{\sigma}_\mu, \sigma_\sigma, \tilde{\sigma}_\sigma$ 
2:  $\mathbf{P}_\mu(0) = \mathbf{0}, \mathbf{P}_\sigma(0) = \mathbf{0}, \omega(0), t = 1$ 
3: for  $B(t) \in \text{data}$  do
4:   (Forward pass)
5:    $\forall x_i \in B(t)$  calculate  $g_{\omega(t)}(x_i)$ 
6:   evaluate the loss  $\mathcal{L}(\omega(t), B(t))$ 
7:   (Backward)
8:   for  $k \in [1 : K]$  do
9:      $\omega_k(t) \leftarrow \omega_k(t-1) - \eta \nabla \mathcal{L}_{\omega_k(t)}$ 
10:  end for
11:  (Tracking with Kalman filter)
12:  for  $k = 1$  do  $K$ 
13:    # Update predicted (a priori) estimate covariances
14:     $\mathbf{P}_\mu(t^-) \leftarrow \mathbf{P}_\mu(t-1) + \sigma_\mu$ 
15:     $\mathbf{P}_\sigma(t^-) \leftarrow \mathbf{P}_\sigma(t-1) + \sigma_\sigma$ 
16:    # Update Kalman Gains
17:     $\mathbf{Q}_\mu \leftarrow \mathbf{P}_\mu(t^-) / (\mathbf{P}_\mu(t^-) + \tilde{\sigma}_\mu)$ 
18:     $\mathbf{Q}_\sigma \leftarrow \mathbf{P}_\sigma(t^-) / (\mathbf{P}_\sigma(t^-) + \tilde{\sigma}_\sigma)$ 
19:    # Update mean
20:     $\mu_k(t^-) \leftarrow \mu_k(t-1) - \eta \nabla \mathcal{L}_{\omega_k(t)}$ 
21:     $\mu_k(t) \leftarrow (1 - \mathbf{Q}_\mu) \mu_k(t^-) + \mathbf{Q}_\mu \omega_k(t)$ 
22:    # Update variance
23:     $\sigma_k^2(t^-) \leftarrow \sigma_k^2(t-1) + \eta^2 (\nabla \mathcal{L}_{\omega_k(t)} - \mu_k(t))^2$ 
24:     $\sigma_k^2(t) \leftarrow (1 - \mathbf{Q}_\sigma) \sigma_k^2(t^-) + \mathbf{Q}_\sigma (\omega_k(t)^2 - \mu_k(t)^2)$ 
25:    # Update (a posteriori) estimate covariances
26:     $\mathbf{P}_\mu(t) \leftarrow (1 - \mathbf{Q}_\mu) \mathbf{P}_\mu(t^-)$ 
27:     $\mathbf{P}_\sigma(t) \leftarrow (1 - \mathbf{Q}_\sigma) \mathbf{P}_\sigma(t^-)$ 
28:  end for
29:  (Time update)
30:   $t \leftarrow t + 1$ 
31: end for

```

by an alternative approach) that we denote $\Sigma(t)$, we simply sample new realizations of $W(t)$ using the following formula:

$$\tilde{\omega}(t) = \boldsymbol{\mu}(t) + \Sigma^{1/2}(t) \times \mathbf{m}_1 \quad (11)$$

in which \mathbf{m}_1 is a realization of the multivariate Gaussian $\mathcal{N}(\mathbf{0}_K, \mathbf{I}_K)$, where $\mathbf{0}_K, \mathbf{I}_K$ are respectively the K -size zero vector and the $K \times K$ size identity matrix.

When we deal with a DNN (the considered case in this paper), we are constrained for tractability reasons to approximate the covariance matrix following the random projection trick proposed in the previous section and we generate new realizations of $W(t)$ as follows:

$$\tilde{\omega}(t) = \boldsymbol{\mu}(t) + \mathbf{R}(\omega(t)) \times \mathbf{m}_2 \quad (12)$$

where $\mathbf{R}(\omega(t))$ is a matrix of size $K \times N$ whose rows $k \in [1, K]$ contain the $\mathbf{r}(\omega_k(t))^\top$ defined in Section 3.2.2. $\mathbf{R}(\omega(t))$ depends on $(\theta_1, \dots, \theta_N)$ and on (ϕ_1, \dots, ϕ_N) defined in Equation 7. \mathbf{m}_2 is a realization of the multivariate Gaussian $\mathcal{N}(\mathbf{0}_N, \mathbf{I}_N)$, where $\mathbf{0}_N, \mathbf{I}_N$ are respectively the zero vector of size N and the identity matrix of size $N \times N$.

Note that since $N \ll K$, computations are significantly accelerated.

Then similarly to works in [31, 22], given input data $(x^*, y^*) \in \mathcal{D}_\tau$ from the testing set, we estimate the marginal likelihood as Monte Carlo integration. First, a sequence $\{\tilde{\omega}^j(t)\}_{j=1}^{N_{\text{model}}}$ of N_{model} realizations of $W(t)$ is drawn (typically, $N_{\text{model}} = 20$). Then, the marginal likelihood of y^* over $W(t)$ is approximated by:

$$\mathcal{P}(y^*|x^*) = \frac{1}{N_{\text{model}}} \sum_{j=1}^{N_{\text{model}}} \mathcal{P}(y^*|\tilde{\omega}^j(t), x^*) \quad (13)$$

For the regression, we use the strategy from [26] to compute the log-likelihood of the regression and consider that the outputs of the DNN applied on x^* are the parameters $\{\mu_{\text{pred}}^j(x^*), (\sigma_{\text{pred}}^j)^2\}_{j=1}^{N_{\text{model}}}$ of a Gaussian distribution (see Section 3.3). Hence, the final output is the result of a mixture of N_{model} Gaussian distributions $\mathcal{N}(\mu_{\text{pred}}^j(x^*), (\sigma_{\text{pred}}^j)^2(x^*))$. During testing, if the DNN has BatchNorm layers, we first update BatchNorm statistics of each of the sampled $\tilde{\omega}^j(t)$ models, where $j \in [1, N_{\text{model}}]$ [19].

4. Experiments

For our implementations we use PyTorch [37]. For evaluation, we use the NLL uncertainty, for classification the accuracy, and for regression we use the MSE $\mathcal{L}_1(t)$ between the predicted and the target outputs. For the out of distribution experiments we use the AUC, AUPR-Success AUPR-Error as in [16].

Unless otherwise specified, we use mini-batches of size 128 and Adam optimizer with fixed learning rate of 0.1 in all our experiments.

4.1. Toy experiments

First we perform a qualitative evaluation of our method on a one-dimensional synthetic dataset generated with a Gaussian Process of zero mean vector and as covariance function an RBF kernel \mathcal{K} with $\sigma^2 = 1$, denoted $GP(\mathbf{0}, \mathcal{K})$. In addition to this process, we add a zero mean Gaussian noise of variance 0.3. We train a neural network composed of one hidden layer and 200 neurons. In Figure 3 we plot the regression estimation provided by TRADI, MC Dropout [9] and Deep Ensembles [26]. Although $GP(\mathbf{0}, \mathcal{K})$ is one of the simplest stochastic processes, results show clearly that the compared approaches do not handle robustly the variance estimation, while TRADI neither overestimates nor underestimates the uncertainty.

4.2. Regression experiments

For the regression task, we consider the experimental protocol and the data sets from [17], and also used in related works [26, 9]. Here, we consider a neural network with one

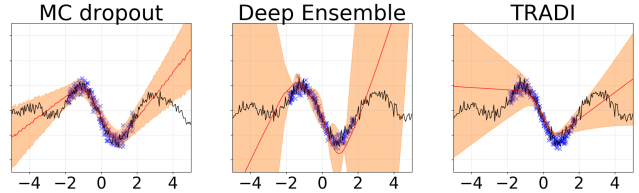


Figure 3: Results on a synthetic regression task with MC dropout, Deep Ensembles and TRADI algorithm. x -axis: spatial coordinate of the Gaussian process. Black lines: ground truth curve. Orange areas: estimated variance. Blue points represents the training points.

hidden layer, composed of 50 hidden units trained for 40 epochs. For each dataset, we do 20-fold cross-validation. For all datasets, we set the dropout rate to 0.1 except for *Yacht Hydrodynamics* and *Boston Housing* for which it is set to 0.001 and 0.005, respectively. We compare against MC Dropout [9] and Deep Ensembles [26] and report results in Table 1. TRADI outperforms both methods, in terms of both RMSE and NLL. Aside from the proposed approach to tracking the weight distribution, we assume that an additional reason for which our technique outperforms the alternative methods resides in the dual training (MSE and NLL) proposed in Section 3.3.

4.3. Classification experiments

For the classification task, we conduct experiments on two datasets. The first one is the MNIST dataset [29], which is composed of a training set containing 60k images and a testing set of 10k images, all of size 28×28 . Here, we use a neural network with 3 hidden layers, each containing 200 neurons, followed by ReLU non-linearities and BatchNorm, and fixed the learning rate $\eta = 10^{-2}$. We share our results in Table 2. For the MNIST dataset, we generate $N_{\text{model}} = 20$ models, in order to ensure a fair comparison with Deep Ensembles. The evaluation underlines that in terms of performance TRADI is positioned between Deep Ensembles and MC Dropout. However, contrarily to Deep Ensembles our algorithm is significantly lighter due to the fact that a single model needs to be trained, while Deep Ensembles approximates the weight distribution by a very costly step of independent training procedures (in this case 20).

We conduct the second experiment on CIFAR-10 [25], with WideResnet 28×10 [47] as DNN. The chosen optimization algorithm is SGD, $\eta = 0.1$ and the dropout rate was fixed to 0.3. Due to the long time necessary for Deep Ensembles to train the DNNs we set $N_{\text{model}} = 15$. Comparative results on this dataset, presented in Table 2, allow us to make similar conclusions with experiments on the MNIST dataset.

Dataset	RMSE			NLL		
	MC dropout	Deep Ensembles	TRADI	MC dropout	Deep Ensembles	TRADI
Boston Housing	2.97 ± 0.85	3.28 ± 1.00	2.84 ± 0.77	2.46 ± 0.25	2.41 ± 0.25	2.36 ± 0.17
Concrete Strength	5.23 ± 0.53	6.03 ± 0.58	5.20 ± 0.45	3.04 ± 0.09	3.06 ± 0.18	3.03 ± 0.08
Energy Efficiency	1.66 ± 0.16	2.09 ± 0.29	1.20 ± 0.27	1.99 ± 0.09	1.38 ± 0.22	1.40 ± 0.16
Kin8nm	0.10 ± 0.00	0.09 ± 0.00	0.09 ± 0.00	-0.95 ± 0.03	-1.2 ± 0.02	-0.98 ± 0.06
Naval Propulsion	0.01 ± 0.00	0.00 ± 0.00	0.00 ± 0.00	-3.80 ± 0.05	-5.63 ± 0.05	-2.83 ± 0.24
Power Plant	4.02 ± 0.18	4.11 ± 0.17	4.02 ± 0.14	2.80 ± 0.05	2.79 ± 0.04	2.82 ± 0.04
Protein Structure	4.36 ± 0.04	4.71 ± 0.06	4.35 ± 0.03	2.89 ± 0.01	2.83 ± 0.02	2.80 ± 0.02
Wine Quality Red	0.62 ± 0.04	0.64 ± 0.04	0.62 ± 0.03	0.93 ± 0.06	0.94 ± 0.12	0.93 ± 0.05
Yacht Hydrodynamics	1.11 ± 0.38	1.58 ± 0.48	1.05 ± 0.25	1.55 ± 0.12	1.18 ± 0.21	1.18 ± 0.39

Table 1: Comparative results obtained on the regression task.

	MNIST		CIFAR-10	
	NLL	ACCU	NLL	ACCU
Deep Ensembles	0.035	98.88	0.173	95.67
MC dropout	0.065	98.19	0.205	95.27
TRADI	0.044	98.63	0.205	95.29

Table 2: Comparative results on a classification task.

		AUC	AUPR Error	AUPR Success
		MNIST\NotMNIST 3Hidden Layers	Deep Ensembles	0.977
	MC dropout	0.8813	0.8975	0.8174
	TRADI	0.9707	0.9842	0.946
CamVid Enet[36]	Deep Ensembles	0.8322	0.5426	0.9401
	MC dropout	0.8024	0.5608	0.8925
	TRADI	0.8326	0.5589	0.9379

Table 3: Comparative results on an out-of-distribution task.

4.4. Uncertainty evaluation for out-of-distribution (OOD) test samples.

In this experiment, we evaluate uncertainty in OOD classes. We consider two datasets, and the objective of these experiments is to evaluate to what extent the trained DNNs are overconfident on instances belonging to classes which are not present in the training set.

First we consider MNIST trained DNNs trained and use them on a test set composed of 10k MNIST images and on an additional NotMNIST dataset containing 19k images representing instances of ten classes of letters. Standard DNNs will assign letter instances of NotMNIST to a number class with high confidence as shown in [1]. For these OOD instances, our approach is able to decrease the confidence as illustrated in Figure 4a, in which we represent the *accuracy vs confidence* curves as in [26].

The *accuracy vs confidence* curve is constructed by considering, for different confidence thresholds, all the test data for which the classifier reports a confidence above the threshold, and then by evaluating the accuracy on this data. The confidence of a DNN is defined as the maximum prediction score. We also evaluate the OOD uncertainty using

AUC, AUPR-Success and AUPR-Error metrics, introduced in [16], and which characterize the quality of the prediction that a testing sample is OOD with respect to the training dataset. We note that TRADI DNN with 20 models provides incorrect predictions on such OOD samples with lower confidence than Deep Ensembles and MC Dropout.

In the second experiment, we train an Enet DNN¹ [36] for semantic segmentation on CamVid dataset [6]. During training, we delete three classes (pedestrian, bicycle, and car), by marking the corresponding pixels as unlabeled. Subsequently, we test with data containing the classes represented during training, as well as the deleted ones. The goal of this experiment is to evaluate the DNN behavior on the deleted classes which represent thus OOD classes. In this experiment we use $N_{\text{model}} = 10$ models trained for 90 epochs with SGD and using a learning rate $\eta = 5 \times 10^{-4}$. In Figures 4b and 4c we illustrate the *accuracy vs confidence* curves and the *calibration* curves [13] for the CamVid experiment. The calibration curve as explained in [13] consists in dividing the test set into bins of equal size according to the confidence, and in computing the accuracy over each bin. Both the calibration and the *accuracy vs confidence* curves highlight whether the DNN predictions are good for different levels of confidence. However, the calibration provides a better understanding of what happens for different scores. The results show that TRADI outperforms the alternative methods in terms of calibration, and that it may provide more reliable confidence scores. Regarding *accuracy vs confidence*, the most significant results for a high level of confidence, typically above 0.7, show how overconfident the network tends to behave; in this range, our results are similar to those of Deep Ensembles. Lastly, in both experiments TRADI obtains the best AUPR-Error, *i.e.*, it performs best in predicting the OOD instances.

Qualitative discussion In Figures 5 and 6 we give as example a scene featuring the three OOD instances of interest (bike, car, pedestrian). Overall, MC Dropout outputs a

¹We specifically select Enet as it is lightweight and allows us to perform a fair comparison with Deep Ensembles.

noisy uncertainty map, but fails to highlight the OOD samples. On the contrary, Deep Ensembles is overconfident, with higher uncertainty values mostly around the borders of the objects. TRADI uncertainty is higher on borders and also on pixels belonging to the actual OOD instances, as shown in the zoomed-in crop of the pedestrian in Figure 6.

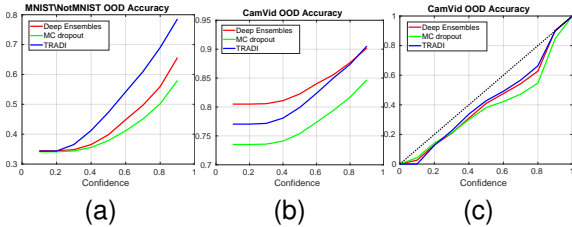


Figure 4: (a) and (b) Accuracy vs confidence plot on the MNIST \ NotMNIST and CamVid experiments, respectively. (c) Calibration plot for the CamVid experiment.

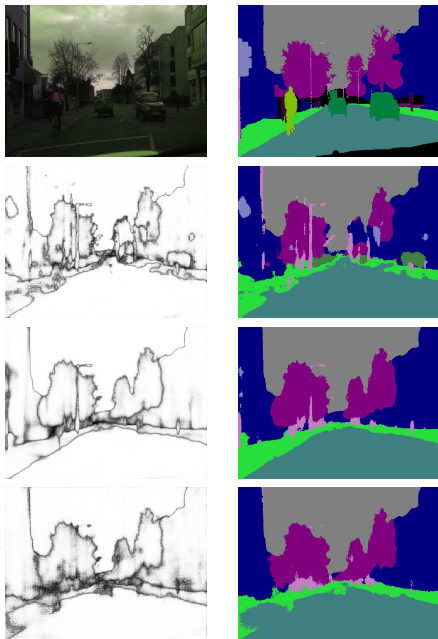


Figure 5: Results on the CamVid experiments. First row: input image and ground truth, second, third and fourth rows: output and confidence score given by MC dropout, Deep Ensembles and our TRADI, respectively.

5. Conclusion

In this work we propose a novel technique for computing the epistemic uncertainty of a DNN. TRADI is simple and easily pluggable in the optimization of any DNN architecture. We show the effectiveness of TRADI over extensive

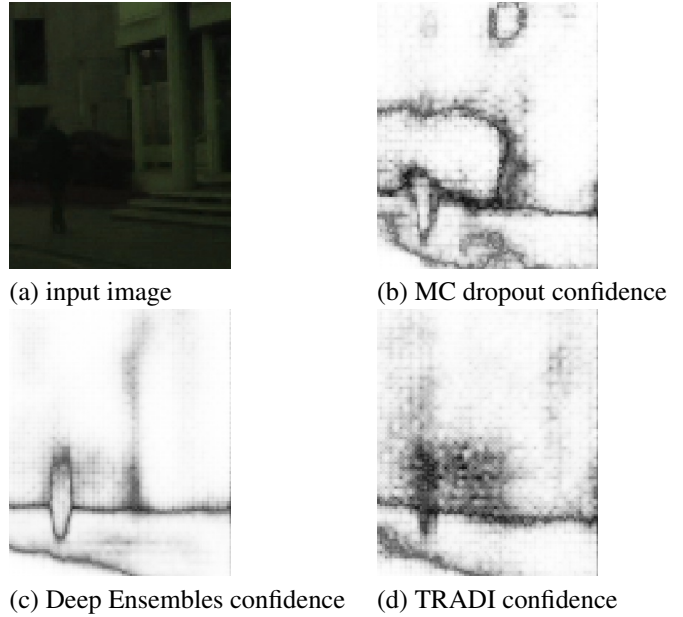


Figure 6: Zooms of the confidence results on the CamVid experiments. In the bottom left of the input image (a), there is a human, hence a pixel region of an unknown class for all the DNNs, since the pedestrian class was amongst the ones marked as unlabeled. Yet, only the TRADI DNN (d) is consistently unconfident.

studies and compare against the popular MC Dropout and the state of the art Deep Ensembles. Our method exhibits an excellent performance on evaluation metrics for uncertainty quantification, and contrarily to Deep Ensembles, for which the training time depends on the number of models, our algorithm does not add any significant cost over conventional training times.

Future works involve extending this strategy to new tasks, *e.g.*, object detection, or new settings, *e.g.*, active learning. Another line of future research concerns transfer learning. So far TRADI is starting from randomly initialized weights sampled from a given Normal distribution. In transfer learning, we start from a pre-trained network where weights are expected to follow a different distribution. If we have access to the distribution of the DNN weights we can improve the effectiveness of transfer learning with TRADI.

Acknowledgments

The authors acknowledge the support of the French National Research Agency (ANR-15-CE39-0005 (ANR MOHICANS)).

References

- [1] Notmnist dataset. <http://yaroslavvb.blogspot.com/2011/09/notmnist-dataset.html>. 7
- [2] Marcin Andrychowicz, Misha Denil, Sergio Gomez, Matthew W Hoffman, David Pfau, Tom Schaul, Brendan Shillingford, and Nando De Freitas. Learning to learn by gradient descent by gradient descent. In *Advances in neural information processing systems*, pages 3981–3989, 2016. 4, 11
- [3] William H Beluch, Tim Genewein, Andreas Nürnberger, and Jan M Köhler. The power of ensembles for active learning in image classification. In *Proceedings of the IEEE Conference on Computer Vision and Pattern Recognition*, pages 9368–9377, 2018. 2
- [4] Charles Blundell, Julien Cornebise, Koray Kavukcuoglu, and Daan Wierstra. Weight uncertainty in neural networks. *arXiv preprint arXiv:1505.05424*, 2015. 2
- [5] Léon Bottou. Stochastic learning. In *Summer School on Machine Learning*, pages 146–168. Springer, 2003. 1
- [6] Gabriel J Brostow, Jamie Shotton, Julien Fauqueur, and Roberto Cipolla. Segmentation and recognition using structure from motion point clouds. In *European conference on computer vision*, pages 44–57. Springer, 2008. 7
- [7] Changhao Chen, Chris Xiaoxuan Lu, Andrew Markham, and Niki Trigoni. Ionet: Learning to cure the curse of drift in inertial odometry. In *The Thirty-Second AAAI Conference on Artificial Intelligence (AAAI-18)*, 2018. 3
- [8] Liang-Chieh Chen, Yukun Zhu, George Papandreou, Florian Schroff, and Hartwig Adam. Encoder-decoder with atrous separable convolution for semantic image segmentation. In *Proceedings of the European conference on computer vision (ECCV)*, pages 801–818, 2018. 3
- [9] Yarin Gal and Zoubin Ghahramani. Dropout as a bayesian approximation: Representing model uncertainty in deep learning. In *international conference on machine learning*, pages 1050–1059, 2016. 1, 2, 6
- [10] Yarin Gal, Jiri Hron, and Alex Kendall. Concrete dropout. In *NIPS*, 2017. 2
- [11] Xavier Glorot and Yoshua Bengio. Understanding the difficulty of training deep feedforward neural networks. In *Proceedings of the thirteenth international conference on artificial intelligence and statistics*, pages 249–256, 2010. 2, 3
- [12] Mohinder S Grewal. *Kalman filtering*. Springer, 2011. 2
- [13] Chuan Guo, Geoff Pleiss, Yu Sun, and Kilian Q Weinberger. On calibration of modern neural networks. In *Proceedings of the 34th International Conference on Machine Learning-Volume 70*, pages 1321–1330. JMLR. org, 2017. 7
- [14] Tuomas Haarnoja, Anurag Ajay, Sergey Levine, and Pieter Abbeel. Backprop kf: Learning discriminative deterministic state estimators. In *Advances in Neural Information Processing Systems*, pages 4376–4384, 2016. 3
- [15] Kaiming He, Xiangyu Zhang, Shaoqing Ren, and Jian Sun. Delving deep into rectifiers: Surpassing human-level performance on imagenet classification. In *Proceedings of the IEEE international conference on computer vision*, pages 1026–1034, 2015. 2, 3, 4, 11
- [16] Dan Hendrycks and Kevin Gimpel. A baseline for detecting misclassified and out-of-distribution examples in neural networks. *arXiv preprint arXiv:1610.02136*, 2016. 6, 7
- [17] José Miguel Hernández-Lobato and Ryan Adams. Probabilistic backpropagation for scalable learning of bayesian neural networks. In *International Conference on Machine Learning*, pages 1861–1869, 2015. 6
- [18] Sergey Ioffe and Christian Szegedy. Batch normalization: Accelerating deep network training by reducing internal covariate shift. *arXiv preprint arXiv:1502.03167*, 2015. 3
- [19] Pavel Izmailov, Dmitrii Podoprikin, Timur Garipov, Dmitry Vetrov, and Andrew Gordon Wilson. Averaging weights leads to wider optima and better generalization. *arXiv preprint arXiv:1803.05407*, 2018. 3, 6
- [20] Rudolph Emil Kalman. A new approach to linear filtering and prediction problems. *Journal of basic Engineering*, 82(1):35–45, 1960. 3, 5
- [21] Alex Kendall, Vijay Badrinarayanan, , and Roberto Cipolla. Bayesian segnet: Model uncertainty in deep convolutional encoder-decoder architectures for scene understanding. *arXiv preprint arXiv:1511.02680*, 2015. 2
- [22] Alex Kendall and Yarin Gal. What uncertainties do we need in bayesian deep learning for computer vision? In *Advances in neural information processing systems*, pages 5574–5584, 2017. 2, 6
- [23] Diederik P Kingma and Jimmy Ba. Adam: A method for stochastic optimization. *arXiv preprint arXiv:1412.6980*, 2014. 1
- [24] Diederik P. Kingma and Max Welling. Auto-encoding variational bayes. In *2nd International Conference on Learning Representations, ICLR 2014, Banff, AB, Canada, April 14-16, 2014, Conference Track Proceedings*, 2014. 2
- [25] Alex Krizhevsky, Geoffrey Hinton, et al. Learning multiple layers of features from tiny images. Technical report, Cite-seer, 2009. 6
- [26] Balaji Lakshminarayanan, Alexander Pritzel, and Charles Blundell. Simple and scalable predictive uncertainty estimation using deep ensembles. In *Advances in Neural Information Processing Systems*, pages 6402–6413, 2017. 1, 2, 3, 5, 6, 7
- [27] John Lambert, Ozan Sener, and Silvio Savarese. Deep learning under privileged information using heteroscedastic dropout. *2018 IEEE/CVF Conference on Computer Vision and Pattern Recognition*, pages 8886–8895, 2018. 2
- [28] Janice Lan, Rosanne Liu, Hattie Zhou, and Jason Yosinski. Lca: Loss change allocation for neural network training. In *Advances in Neural Information Processing Systems*, pages 3614–3624, 2019. 3
- [29] Yann LeCun, Léon Bottou, Yoshua Bengio, Patrick Haffner, et al. Gradient-based learning applied to document recognition. *Proceedings of the IEEE*, 86(11):2278–2324, 1998. 6
- [30] Chao Liu, Jinwei Gu, Kihwan Kim, Srinivasa G Narasimhan, and Jan Kautz. Neural rgb (r) d sensing: Depth and uncertainty from a video camera. In *Proceedings of the IEEE Conference on Computer Vision and Pattern Recognition*, pages 10986–10995, 2019. 3

- [31] Wesley Maddox, Timur Garipov, Pavel Izmailov, Dmitry Vetrov, and Andrew Gordon Wilson. A simple baseline for bayesian uncertainty in deep learning. *arXiv preprint arXiv:1902.02476*, 2019. 1, 3, 6
- [32] Jishnu Mukhoti and Yarin Gal. Evaluating bayesian deep learning methods for semantic segmentation. *CoRR*, abs/1811.12709, 2018. 2
- [33] Radford M. Neal. *Bayesian Learning for Neural Networks*. Springer-Verlag, Berlin, Heidelberg, 1996. 2
- [34] Ian Osband. Risk versus uncertainty in deep learning : Bayes , bootstrap and the dangers of dropout. 2016. 2
- [35] Ian Osband, John Aslanides, and Albin Cassirer. Randomized prior functions for deep reinforcement learning. In *NeurIPS*, 2018. 2
- [36] Adam Paszke, Abhishek Chaurasia, Sangpil Kim, and Eugenio Culurciello. Enet: A deep neural network architecture for real-time semantic segmentation. *arXiv preprint arXiv:1606.02147*, 2016. 7
- [37] Adam Paszke, Sam Gross, Francisco Massa, Adam Lerer, James Bradbury, Gregory Chanan, Trevor Killeen, Zeming Lin, Natalia Gimelshein, Luca Antiga, et al. Pytorch: An imperative style, high-performance deep learning library. In *Advances in Neural Information Processing Systems*, pages 8024–8035, 2019. 6
- [38] A. Rahimi and B. Recht. Random features for large-scale kernel machines. In *Advances in neural information processing systems*, pages 1177–1184, 2007. 4
- [39] Tim Salimans and Durk P Kingma. Weight normalization: A simple reparameterization to accelerate training of deep neural networks. In *Advances in Neural Information Processing Systems*, pages 901–909, 2016. 3
- [40] Nitish Srivastava, Geoffrey Hinton, Alex Krizhevsky, Ilya Sutskever, and Ruslan Salakhutdinov. Dropout: A simple way to prevent neural networks from overfitting. *J. Mach. Learn. Res.*, 15(1):1929–1958, Jan. 2014. 2
- [41] Mattias Teye, Hossein Azizpour, and Kevin Smith. Bayesian uncertainty estimation for batch normalized deep networks. In *ICML*, 2018. 2
- [42] Tijmen Tieleman and Geoffrey Hinton. Lecture 6.5-rmsprop: Divide the gradient by a running average of its recent magnitude. *COURSERA: Neural networks for machine learning*, 4(2):26–31, 2012. 1
- [43] Guangrun Wang, Jiefeng Peng, Ping Luo, Xinjiang Wang, and Liang Lin. Batch kalman normalization: Towards training deep neural networks with micro-batches. *arXiv preprint arXiv:1802.03133*, 2018. 3
- [44] Christopher KI Williams and Carl Edward Rasmussen. *Gaussian processes for machine learning*, volume 2. MIT press Cambridge, MA, 2006. 4
- [45] Greg Yang. Scaling limits of wide neural networks with weight sharing: Gaussian process behavior, gradient independence, and neural tangent kernel derivation. *arXiv preprint arXiv:1902.04760*, 2019. 4, 11
- [46] Fisher Yu, Vladlen Koltun, and Thomas Funkhouser. Dilated residual networks. In *Proceedings of the IEEE conference on computer vision and pattern recognition*, pages 472–480, 2017. 3
- [47] Sergey Zagoruyko and Nikos Komodakis. Wide residual networks. *arXiv preprint arXiv:1605.07146*, 2016. 6

TRADI: Tracking deep neural network weight distributions (Supplementary material)

6. TRACKING OF THE DISTRIBUTION (TRADI) OF WEIGHTS OF A NEURAL NETWORK

In this section, we append to section 3.2.1 of the main paper a part in which we explain how to track the covariance matrix of a shallow neural network and 3.4 on the main article by explaining how we choose the parameters of TRADI.

6.1. TRACKING THE MEAN AND VARIANCE OF THE WEIGHTS AND THE COVARIANCE

We consider a neural network (NN) for which each layer has few neurons, less than 100. Our goal here is to estimate, for all weights $\omega_k(t)$ of the NN and at each time step t of the training process, $\mu_k(t)$ and $\sigma_k^2(t)$ the parameters of their normal distribution. Furthermore, we want to estimate $\Sigma_{k,k'}(t)$ which is the covariance matrix between the $\omega_k(t)$ and $\omega_{k'}(t)$. Note that, since we assume that weights on different layers are independent, we evaluate the covariance for k, k' belonging to the same layer, otherwise their covariance is null. To this end, we leverage mini-batch SGD to optimize the loss between two weight realizations.

The derivative of the loss with respect to a given weight $\omega_k(t-1)$ over a mini-batch $B(t)$ is given by:

$$\nabla \mathcal{L}_{\omega_k(t)} = \frac{1}{|B(t)|} \sum_{(x_i, y_i) \in B(t)} \frac{\partial \mathcal{L}(\omega(t-1), y_i)}{\partial \omega_k(t-1)} \quad (\text{S1})$$

Weights $\omega_k(t)$ are then updated as follows:

$$\omega_k(t) = \omega_k(t-1) - \eta \nabla \mathcal{L}_{\omega_k(t)} \quad (\text{S2})$$

The weights of NNs are randomly initialized at $t = 0$ by sampling $W_k(0) \sim \mathcal{N}(\mu_k(0), \sigma_k^2(0))$, where the parameters of the distribution are set empirically on a per-layer basis as in [15]. In addition, for all couples of weights (k, k') , the corresponding element of the covariance matrix is given by $\Sigma_{k,k'}(0) = 0$ since all the weights are considered independent at time $t = 0$.

Similarly with the main article, we use the following state and measurement equations for the mean $\mu_k(t)$:

$$\begin{cases} \mu_k(t) = \mu_k(t-1) - \eta \nabla \mathcal{L}_{\omega_k(t)} + n_\mu \\ \omega_k(t) = \mu_k(t) + \tilde{n}_\mu \end{cases} \quad (\text{S3})$$

where n_μ is the state noise, and \tilde{n}_μ the observation noise, realizations of $\mathcal{N}(0, \sigma_\mu^2)$ and $\mathcal{N}(0, \tilde{\sigma}_\mu^2)$ respectively. The state and measurement equations for the variance σ_k are given by:

$$\begin{cases} \sigma_k^2(t) = \sigma_k^2(t-1) + (\eta \nabla \mathcal{L}_{\omega_k(t)})^2 - \eta^2 \mu_k(t)^2 + n_\sigma \\ z_k(t) = \sigma_k^2(t) - \mu_k(t)^2 + \tilde{n}_\sigma \\ \text{with } z_k(t) = \omega_k(t)^2 \end{cases} \quad (\text{S4})$$

where n_σ is the state noise, and \tilde{n}_σ is the observation noise, realizations of $\mathcal{N}(0, \sigma_\sigma^2)$ and $\mathcal{N}(0, \tilde{\sigma}_\sigma^2)$ respectively. As proposed in the main article, and similarly with [2, 45], we assume that weights during back-propagation and forward pass are independent. We then get:

$$\begin{aligned} \Sigma(t)_{k,k'} &= \Sigma(t-1)_{k,k'} + \\ &\eta^2 \mathbb{E} [\nabla \mathcal{L}_{\omega_k(t)} \nabla \mathcal{L}_{\omega_{k'}(t)}] - \eta^2 \mathbb{E} [\nabla \mathcal{L}_{\omega_k(t)}] \mathbb{E} [\nabla \mathcal{L}_{\omega_{k'}(t)}] \end{aligned} \quad (\text{S5})$$

This leads to the following state and measurement equations for the covariance $\Sigma(t)_{k,k'}$:

$$\begin{cases} \Sigma(t)_{k,k'} = \Sigma(t-1)_{k,k'} + (\eta^2 \nabla \mathcal{L}_{\omega_k(t)} \nabla \mathcal{L}_{\omega_{k'}(t)}) \\ \quad - \eta^2 \mu_k(t) \mu_{k'}(t) + n_\Sigma \\ l_{k,k'}(t) = \Sigma(t)_{k,k'} - \mu_k(t) \mu_{k'}(t) + \tilde{n}_\Sigma \\ l_{k,k'}(t) = \Sigma(t)_{k,k'} - \mu_k(t) \mu_{k'}(t) + \tilde{n}_\Sigma \end{cases} \quad (\text{S6})$$

where n_Σ is the state noise and \tilde{n}_Σ is the observation noise, realizations of $\mathcal{N}(0, \sigma_\Sigma^2)$ and $\mathcal{N}(0, \tilde{\sigma}_\Sigma^2)$ respectively.

6.2. TRADI PARAMETERS

We've set the number of random projections $N = 10$ in all experiments in order to get a fast approximation of the covariance matrix. We validated this choice experimentally and noticed that the performance is similar for larger values of N . $N = 10$ ensures a relatively low computational cost. We used $\sigma_{\text{rbf}} = 1$ for the RBF parameter of the random projection. We have tested different values, without substantial changes in the results. As it can be seen in the algorithm section we have performed a weighted average between the estimated variance/mean with the tracked variance/mean, where the weight depends on Kalman gain.

7. COMPLEMENTARY RESULTS

In this section, we detail some of the results reported in the main article for the OOD experiments. The major interest of OOD experiments is that they allow one to see how much we can rely on a DNN. This question is also crucial for industrial research. In this scenario, a particular DNN is trained for a specific application/context which takes into account a certain number of classes. However, in the testing phase new unforeseen objects may appear, potentially leading to wrong/dangerous decisions if the DNN confidence is badly calibrated.

7.1. Results on MNIST

Figure S1 shows the calibration plots for the OOD experiments with MNIST and NotMNIST datasets. As one can see, our strategy (blue curve) has better performances on predicting OOD classes. Calibration plots can easily show whether a DNN is overconfident or not and give an idea on how reliable are the predictions of the DNN. From these plots we see that Deep Ensembles and MC dropout are overconfident, hence they classify non-digits with wrong classes and with high confidence. Our strategy is therefore more suitable for this problem, although still improvable in the lower confidence ranges.

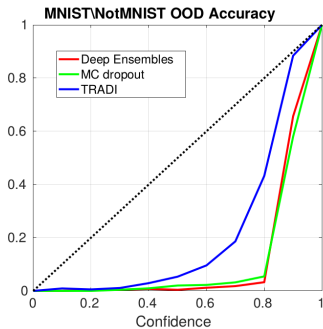


Figure S1: Calibration plot for MNIST \ NotMNIST.

7.2. Results on CamVid

We provide additional scores for CamVid experiments. In Figure S2b we illustrate the average precision calibration curve. This curve is similar to the calibration plot, with the different that for each confidence bin, we do not plot the accuracy but the average precision. The usefulness of the precision is that it highlights more the false-positive effects than the accuracy. We observe in in Figure S2 that TRADI is better on both measures at identifying OOD classes.

In Table 1 we report the mIoU and the global accuracy scores. On these metrics, TRADI is between Deep Ensembles and MC Dropout. In contrast to Deep Ensembles we do not need to train multiple DNNs. In order to achieve good performances on semantic segmentation for complex urban scenes, high capacity DNNs are necessary. Training multiple instances of such networks as in Deep Ensembles brings a significant computational cost. Furthermore, these models are usually updated when new data is recorded and each time the full ensemble needs updating. TRADI requires training a single network each time.

In Figures S4, S5, S6, and S7 we report additional qualitative results. Figures S6 and S7 show zoom-in over areas of interest in Figures S4 and S5 respectively. We provide the color code for the semantic segmentation map in Fig-

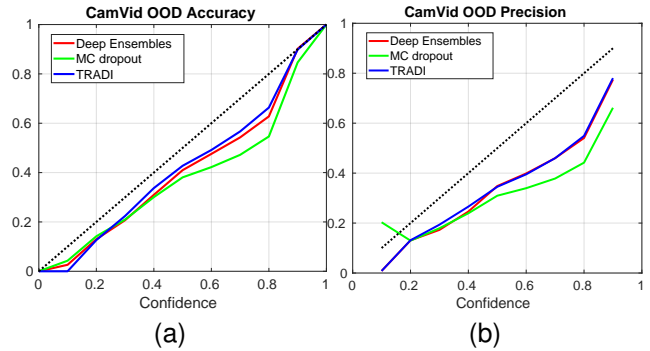


Figure S2: (a) Calibration plot for the CamVid experiment. (b) Calibration plot, where on the Y axis we replace the Accuracy by the average precision of each class for the CamVid experiment.

	MC dropout	Deep Ensembles	TRADI
mean IoU	0.4857	0.5719	0.5298
Accuracy	0.8034	0.8806	0.8488

Table 1: CamVid semantic segmentation results (mIoU, accuracy).

ure S3. We remind that in this experiments the classes human, bicyclist, and car are used as OOD and removed from the train set. We can see that TRADI outputs less confident predictions for human pixels, comparing to Deep Ensembles and MC Dropout.

Comparing with Deep Ensembles. Deep Ensembles is among the most powerful and effective techniques for epistemic uncertainty. However few works on uncertainty estimation with DNNs on computer vision tasks have considered it for evaluation. We argue that this work is one of the first to truly challenge Deep Ensembles. While we do not achieve higher accuracy than Deep Ensembles, our approach strikes a good compromise between computational cost for training and prediction performance. The computational budget for Deep Ensembles is proportional to the number of models in the ensemble, while for TRADI we always train a single model regardless of the number of network samples we have at test time. Our results on the OOD experiments challenge and sometimes outperform the Deep Ensembles ones.



Figure S3: Color map for the CamVid experiment.

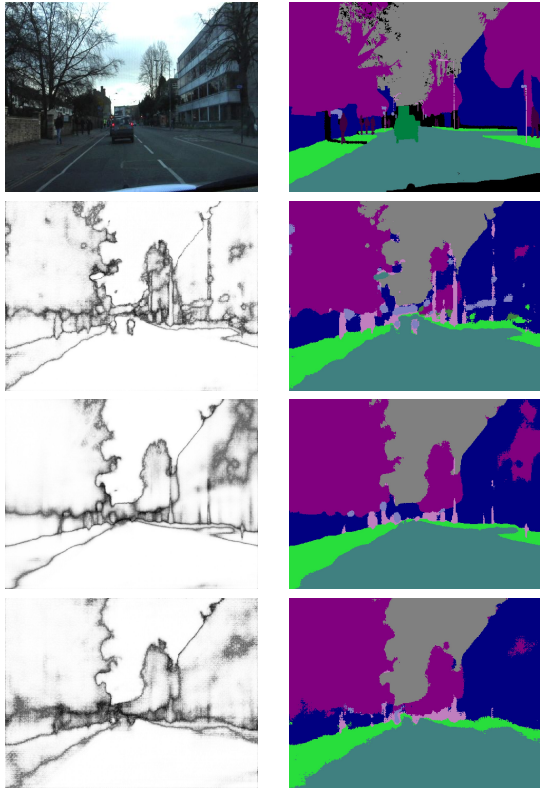


Figure S4: Results on the CamVid experiments. First row: input image (the image contrast has been enhanced for clarity with respect to the original dataset image) and ground truth, second, third and fourth rows: output and confidence score given by MC dropout, Deep Ensembles and our TRADI method, respectively.

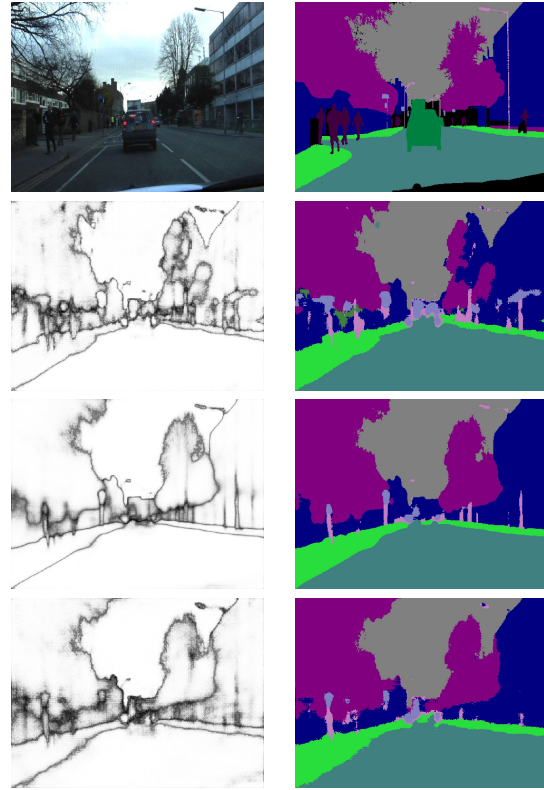


Figure S5: Results on the CamVid experiments. First row: input image (the image contrast has been enhanced for clarity with respect to the original dataset image) and ground truth, second, third and fourth rows: output and confidence score given by MC dropout, Deep Ensembles and our TRADI method, respectively.

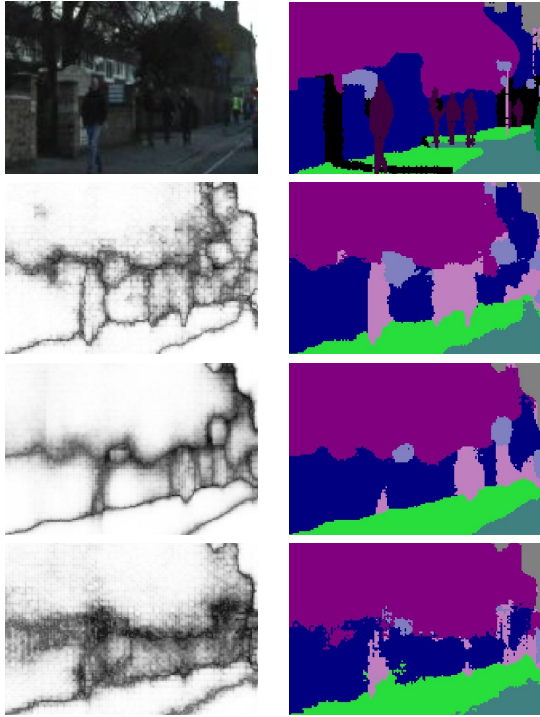


Figure S6: Zooms of the confidence results on the CamVid experiments. First row: input image (the image contrast has been enhanced for clarity with respect to the original dataset image) and ground truth, second, third and fourth rows: output and confidence score given by MC dropout, Deep Ensembles and our TRADI method, respectively.

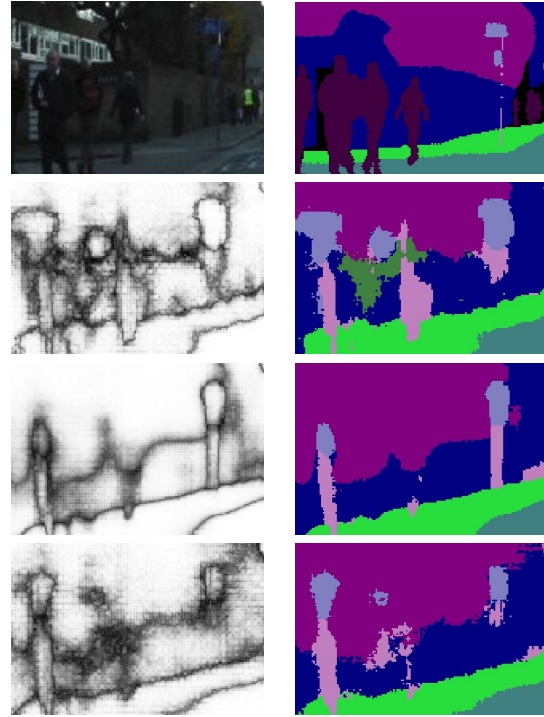


Figure S7: Zooms of the confidence results on the CamVid experiments. First row: input image (the image contrast has been enhanced for clarity with respect to the original dataset image) and ground truth, second, third and fourth rows: output and confidence score given by MC dropout, Deep Ensembles and our TRADI method, respectively.